Physica Medica 60 (2019) 7–13

Contents lists available at ScienceDirect

Physica Medica

journal homepage: www.elsevier.com/locate/ejmp

Original paper

Radio-sensitization efficacy of gold nanoparticles in inhalational nanomedicine and the adverse effect of nano-detachment due to coating inactivation

Sherif M. Gadoue[a,*], Dolla Toomeh[b]

[a] Department of Physics and Applied Physics, University of Massachusetts Lowell, Lowell, MA 01854, USA
[b] Department of Radiation Oncology, University of Washington School of Medicine, Seattle, WA 98195, USA

ARTICLE INFO

Keywords:
Gold nanoparticles
Radiotherapy
Coating inactivation
Lung cancer

ABSTRACT

Gold nanoparticles (GNPs) are an emerging area of interest in radiation therapy due to their unique radio-sensitizing properties. In the literature, the enhancing capability of GNPs is usually quantified using the metric dose enhancement ratio (DER). Traditionally, the focus of the vast majority of studies has always been on intravenous administration of GNPs. However, recent work showed the potential of using GNP inhalation, rather than intravenous injection, to enhance the dose to the lung. Yet, some of these studies are employing simplistic analytical methods to calculate DER and, thus far, there are no detailed computations of the enhancement profiles therein. Moreover, the coating on the GNP surface can be adversely affected by the large gradient of the radiation dose in the immediate vicinity of GNPs, leading to the rupture of ligands and detachment of GNPs from the surface of the membrane, and hence the loss of its efficacy. In this study, a next-generation deterministic code was used to resolve the DER profile at the interface between the septum, air, and surface of GNPs when they are attached and detached. The results show that the large values of DER in conjunction with the developed hot spots are very effective in lung treatment; on the other hand, coating rupture can lead to significant reduction in DER that may reach 64%. Thus, GNPs can be beneficial in inhalational medicine to treat lung cancer, provided that more comprehensive studies on the characteristics of the coating are addressed to maximize the radio-therapeutic benefit of GNPs.

1. Introduction

According to recent statistics, lung cancer is the leading cause of cancer death in the US (27% for males and 25% for females) with an average five-years survival rate of 19% [1]. It has been shown that increasing the survival rate can be achieved by delivering higher doses of radiation [2]. Machaty et al. have demonstrated that an increase in the biologically equivalent dose will be translated into a decreased risk of lung cancer death [3]. As lung is close to critical organs, the high levels of radiation dose delivered should be appropriately accompanied with sparing of the surrounding healthy tissue; a task which is highly challenging. One way to achieve this is by using respiratory motion management techniques; nonetheless, tumor size variations between treatment fractions could lead to large errors, and considerably high doses to healthy tissues [2]. An alternative way to increase the local radio-therapeutic dose, while leveraging the primary radiation level incident on the patient, is to use smart fiducials loaded with graphene oxide nano-flakes [4], regular [5–14] or multifunctional nanoparticles [15].

Nanoparticles exhibit unique properties that make them highly suited to numerous medical radiation applications. Their distinctive physicochemical properties, such as particle size, surface area, shape, and chemical composition render them ideal candidates as cancer therapeutic agents. It is important to note that these properties have a great impact on the aggregation state, cellular uptake, nanotoxicity, endocytosis process and radiosensitizing effects of nanoparticles [16–23]. Moreover, they have potential for cancer imaging [24], spectroscopic detection and photothermal therapy, as a result of their prominent electrical and optical properties, such as quantum confinement and surface plasmon resonance [25]. Nanoparticles can be synthesized using one of two classes, bottom-up or top-down [26,27]. In the top-down (destructive) class, a larger molecule is reduced into smaller units that can be converted to nanometric scale particles. Among the most widely used methods in this approach are the

* Corresponding author.
E-mail address: smgadoue@gmail.com (S.M. Gadoue).

https://doi.org/10.1016/j.ejmp.2019.02.013
Received 10 April 2018; Received in revised form 21 January 2019; Accepted 15 February 2019
Available online 21 March 2019

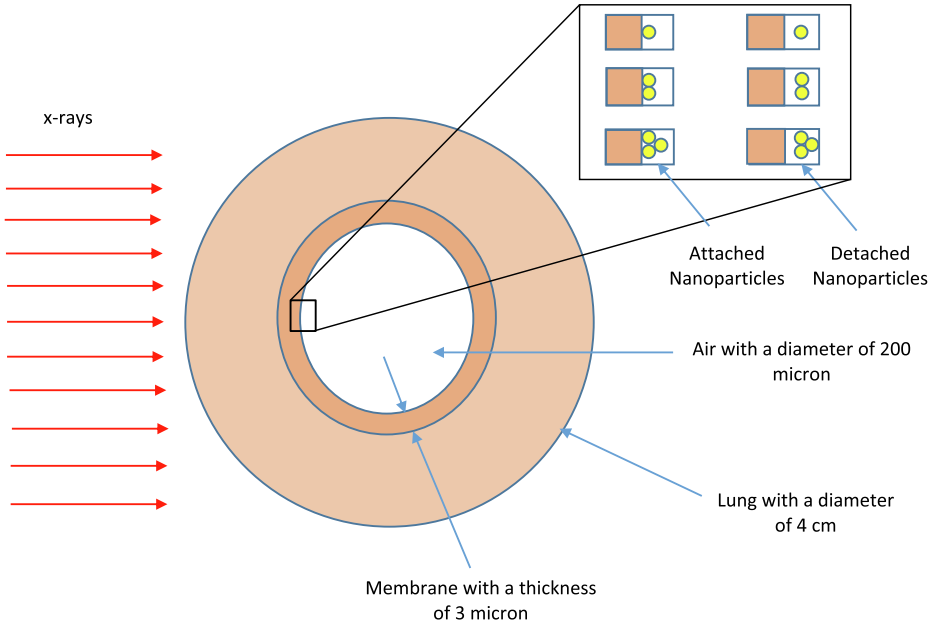

Fig. 1. Schematic of the geometry of the problem, dimensions are not to scale.

mechanical milling, laser ablation, and thermal decomposition. While in the bottom-up (constructive) category, nanoparticles are formed from relatively smaller entities using techniques such as sol gel, spinning, and biochemical synthesis [26–28].

In the context of lung dose escalation, nanoparticles-aided radiotherapy represents a highly efficient way to significantly amplify the energy deposition in the particle's nanometric vicinity, while maintaining a minimal dose to healthy surroundings [6,10]. When exposed to diagnostic x-rays, gold nanoparticles (GNPs) emit a significant number of photoelectrons, due to the increased cross section of gold for this particular interaction at this energy range [6]. The vacancy in the gold atom is then filled by electrons from higher energy levels, and the difference in energy is emitted by the atom in the form of x-rays or by releasing Auger electron(s). Having low energies, Auger electrons leaking from GNP will deposit their energy locally in the tumor. This will result in an amplification of the dose deposited around GNP, the metric dose enhancement ratio (DER) is invariably used throughout the literature to quantify this relative increase.

GNPs can be introduced into the body through several pathways [29]. The major and most widely administration is by intravenous injection [30], which has many limitations due to several factors. One important factor resides in the GNPs size which is comparable to small viruses and proteins. As a result, the presence of GNPs in the body might stimulate the immune system, which will lead to induced immuno-toxicity [28,30]. In addition, the injection of GNPs in the bloodstream may induce blood clotting, or result in breaking blood cells that can lead to hemoglobin release; phenomena known by hemolysis [28]. Moreover, GNPs are responsible for hepatic and splenic toxicity, due to their increased accumulation in the liver and spleen [31]. Many *in-vivo* experiments in mice showed that the accumulation of nanoparticles leads to cellular damage and acute inflammation in the liver [32].

Administration of GNPs via inhalation would overcome the aforementioned complications [33–36]. It can be advantageous over the injection method in several ways: the possibility of administration of higher concentrations [36,37], the rapid action [33], the noninvasive nature of administration, and the prevention of liver toxicity [34]. However, the size of the particle may cause the translocation into the systemic circulation through lung capillaries [34,38].

Hao et al. studied the DER of inhaled nanoparticles of different types: gold, carboplatin, and cisplatin when administered by inhalation route [35]. By comparing their results to the DER from intravenous injection, they concluded that the administration via inhalation could lead to a significant increase in DER in the tumor.

Further, and as pointed out in the work of Gadoue et al. [7], a considerable amount of dose gradient is located in the region surrounding the GNP which may, in some situations, affect the chemical bonds in the coating. As a consequence, GNPs may detach from the surface and, hence, will lose its enhancing power.

In this paper, the radiation transport code, Sandia Computational Engine for Particle Transport for Radiation Effects (SCEPTRE), is used to calculate the DER due to different GNPs patterns inhaled in the lung. Two scenarios are considered, first when GNPs are attached to the septum and, second, when they are shifted from the surface of the septic membrane by a distance of 100 nm. In both cases, x-rays generated at 120 kVp are used as representative of the theranostic (or diagnostic) energy beams.

2. Methods

2.1. Model and geometry

The lung is a highly complex organ consisting of innumerable "patches" of air and soft tissue of highly varying dimensions, with a large number of air-tissue interfaces [39]. In order to obtain realistic results from GNP simulation in this unique organ, it is necessary to establish a reasonable model. The model used in this study considers the whole lung as one entity having a homogenized (averaged over tissue and air) physical density. In the center of the homogenized portion, a small microscopic region is used to be representative of an alveolus where gas exchange takes place. The alveolus is comprised of an air sac within which the inhaled GNPs become attached to the septic membrane that separates adjacent alveoli.

A detailed comprehension of the physico-chemical interactions of synthesized GNPs, on the biological level, is apparently necessary for the engineering of optimal GNPs for radiosensitization [40]. GNPs can be prepared using the classical citrate reduction method, in which Au (III) aqueous solution is chemically reduced by citrate ions. 2 ml of 1% sodium citrate water solution is added to 20 ml of $HAuCl_4$ water solution (1 mM) near the boiling point and stirred for 10 min. The size and shape of GNPs are the most important factors that dictate the amount of internalization [16,40]. In this study, 100 nm diameter spherical

Table 1
The elemental composition of soft tissue, air and homogenized lung tissue used in the simulation.

Material/ composition	Soft tissue (1.00 g/cm^3)	Air (0.001205 g/ cm^3)	Homogenized lung tissue (0.26 g/cm^3)
hydrogen	10.45%	–	10.30%
carbon	23.22%	0.01%	10.50%
nitrogen	2.49%	75.53%	3.10%
oxygen	63.02%	23.18%	74.90%
sodium	0.11%	–	0.20%
magnesium	0.01%	–	–
phosphorus	0.13%	–	0.20%
sulfur	0.20%	–	0.30%
chlorine	0.13%	–	0.30%
potassium	0.20%	–	0.20%
calcium	0.02%	–	–
iron	0.01%	–	–
argon	–	1.28%	–

nanoparticles are considered, and the composition is assumed to consist of pure gold.

The geometry of the problem, as depicted in Fig. 1, consists of an outer sphere of 2 cm radius representing the homogenized lung tissue with a density of 0.26 g/cm^3. Within the outer sphere, a spherical shell of 3 μm thickness (septum membrane) encloses an inner sphere of radius 100 μm consisting of only air that represents the alveolar sac. Different patterns of GNPs are examined; a single GNP, two and three GNPs attached to the membrane. The same patterns are studied when GNPs are separated from the membrane by a distance of 100 nm. X-ray photons generated at 120 kVp are incident on the outer sphere from the left in parallel plane direction.

The detailed elemental composition (by weight fraction) of soft tissue, air [41], and homogenized lung tissue [42] used in the simulation are listed in Table 1.

2.2. Simulations

It is important to recognize that the secondary electron emission from the surface of GNP exhibits an angular dependence [7,43]. Conveniently, for each spherical shell surrounding GNP, the dose deposited should be calculated as a function of angle, rather than averaged over the whole shell (this is especially critical when the spherical shell encompasses more than one material of different properties). Preferably, deterministic radiation transport codes are well suited for such burdensome computations at the nano-scale.

The coupled photon-electron radiation transport code SCEPTRE version 1.7, developed by Sandia National Laboratories, was used to perform the deterministic computations. SCEPTRE solves different forms of the steady state Boltzmann radiation transport equation, using finite element methods. Various angular treatments such as the discrete ordinates and the spherical harmonics methods are provided. Like many other deterministic packages, the multigroup formalism is used to discretize the energy domain. First order sweeping algorithms and different Krylov solvers are also available. More details about solution algorithms implemented in SCEPTRE can be found elsewhere [44,45]. The angular method used in the calculations is the discrete ordinates S_{16}, 50 linear photon and 50 logarithmic electron energy groups were used with convergence tolerance of 10^{-8}. The cross sections are generated using the coupled electron-photon cross-section code CEPXS, available in the integrated tiger series (ITS) code package, with a lower energy cutoff of 1 keV.

To evaluate the enhancement capability of GNPs, it is customary to use the DER metric which is defined as:

$$\mathrm{DER} = \frac{\text{dose delivered to the medium in the presence of GNP}}{\text{dose delivered to the medium in the absence of GNP}} \quad (1)$$

The calculation of the DER profile for each case involves two runs; in the first one, the material of GNP in the input file is set to gold (regular run), while in the second run the material is replaced by air as if GNP(s) do not exist. For both runs, the dose is calculated for all mesh elements in the geometry, the resulting datasets are then divided element by element to obtain the DER. The DER profiles are visualized using color-coded plots, the color code scale is determined by the maximum and minimum value of the DER in the region of interest (ROI) with GNP(s) excluded. Each case has its own color code range rather than a unified range for better visualization of the fine details of the individual distributions. The color code scheme is chosen so that the highest values of DER in the ROI are red and orange, such regions are referred to, in this study, by "hot spots". Most of the results are given on the X-axis along which photons are incident and, therefore, is the axis of anisotropy.

Moreover, in order to quantify the percentage loss of DER due to GNP detachment from the membrane, the following formula is used:

$$\text{Percentage loss in DER} = \frac{\mathrm{DER(attached)} - \mathrm{DER(detached)}}{\mathrm{DER(attached)}} * 100\% \quad (2)$$

3. Results

Fig. 2 illustrates DER profiles due to the three GNP arrangements attached to the septum membrane, following radiation exposure of x-rays. The thickness of the septum shown in the figure is 300 nm. Within the membrane, the overall shape of the DER profile exhibits a semi-circular morphology. As can be seen from the results, there exist hot spot regions whose value is dictated by the number of GNPs involved, and location is determined based on whether GNP is single or clustered. For example, in the case of one GNP, the hot spot area has a maximum DER value of 9.998 in the region of the membrane contiguous with the GNP along the photons incidence axis (x-axis). In general, the secondary electron emission probability from the surface of GNP in the

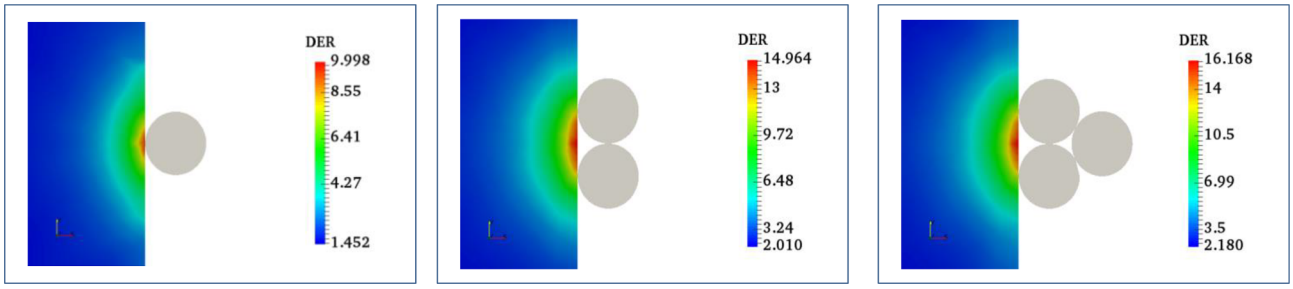

Fig. 2. DER profiles for a membrane thickness of 300 nm due to different GNP patterns attached to the septum membrane, x-ray photons generated at 120 kVp are incident from the left.

180° direction is the lowest, and there are polar angles, in the reverse direction, proximal to the incident x-rays, that exhibit relatively higher emission probability, as indicated by Gadoue et al. [7]. Nevertheless, a non-negligible fraction of the electrons emitted at angles of maximum emission is lost in the air before reaching the surface of the membrane, unlike the electrons emitted in the differential solid angle around 180° direction where there is little or no electron loss in air.

For the case of two GNPs, the maximum DER value of the hot spot is 14.964 in the region of the membrane around the line passing by the point of tangency of the two GNPs. Here, the hot spot is developed by the additive effect of secondary electrons emitted from the lower portion of the top GNP, and the upper part of the bottom GNP traveling toward the hot spot area. Likewise, for the case of three GNPs, the hot spot region is formed in a similar fashion with an additional contribution, due to the secondary electrons (from the extra GNP to the right of the ensemble) that manage to pass through air and the other two GNPs in the direction of the membrane.

Essentially, the hot spot area corresponding to the pattern of two and three GNPs is wider compared to that developed in the case of one GNP. This is not surprising since the underlying mechanism of hot spot formation is closely associated with the additive effects. Needless to say is that the values of DER in general, and hot spots in particular, are the highest for the pattern of three GNPs, whilst it is slightly lower for the case of two GNPs, and the lowest for one GNP.

Fig. 3 depicts the situation of GNPs detachment from the membrane and the resulting effect on the DER profiles for the different GNPs patterns under investigation. The thickness of the region of the septum shown is again 300 nm. From the figure, it can be seen that the values of DER have been significantly reduced as compared to the corresponding values in the attached case for all GNP patterns. In addition, the overall DER profile shape within the septum membrane has been altered with some obvious irregularities. Similar to the attached case, the pattern of three GNPs exhibits the highest values of DER, followed by a slight decrease in the case of two GNPs, and the lowest is for one GNP.

It is important to note that the anisotropy effects are highly evident. For instance, in the case of one GNP, minute hot spots (in yellow) can be seen on the surface of the membrane above and below the central red hot spot region. In addition, the main hot spot area is deformed by the receding contribution of electrons coming from the reverse 180 direction.

Fig. 4a shows the values of DER for all patterns of GNPs, attached and detached from the septum, along the x-axis and for a distance of 300 nm within the membrane. It is obvious that all DER profiles rapidly fall off and reach values of roughly two after 300 nm, due to the short term effects of Auger electrons. Interesting to note is the fact that for the first 25 nm within the membrane, the DER for one attached GNP is higher than it is for an agglomerate of even three detached GNPs (the difference is roughly from two to three). Moreover, the DER profile of the detached GNPs lacks the steep dose gradient characteristic of GNPs. Beyond 25 nm, the difference shrinks to values equal to or less than one. It is worth noting that higher values of DER are far more effective than their lower counterparts in terms of biological impact, even if they are

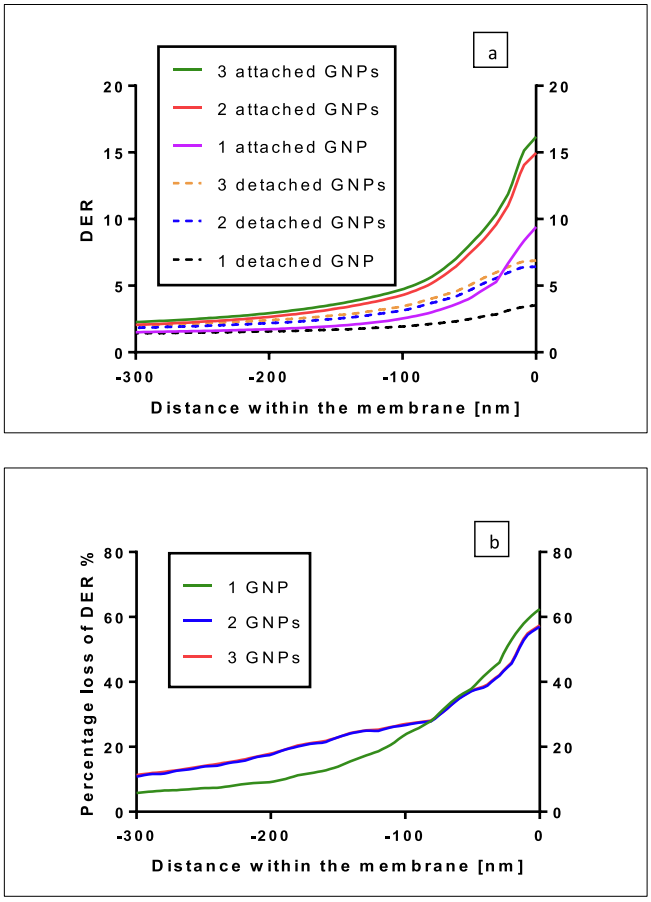

Fig. 4. (a) The values of DER for all examined GNPs patterns along the x-axis from the surface of the membrane up to a distance of 300 nm, x-rays are incident from the left and GNPs are to the right of the plot. (b) The percentage loss of DER for all GNPs patterns.

extending over shorter distances. Therefore, it can be concluded, to a certain degree of approximation, that the efficacy of one attached GNP is superior to that of two or three detached GNPs; a fact that introduces the important concept of degradation of enhancing power due to GNP detachment.

Fig. 4b shows the percentage of such loss of enhancement for the three cases. According to the figure, the percentage loss in the enhancing power is nearly similar for the case of two and three GNPs, whilst it is slightly higher for one GNP in the first 50 nm within the membrane. For example, the maximum percentage loss for one GNP is 62.46%, while for two GNPs it is 57.06%, and for three the percentage is 57.41%. However, the percentage loss for all cases will approach almost 10% after around 300 nm due to the diminished contribution of Auger electrons.

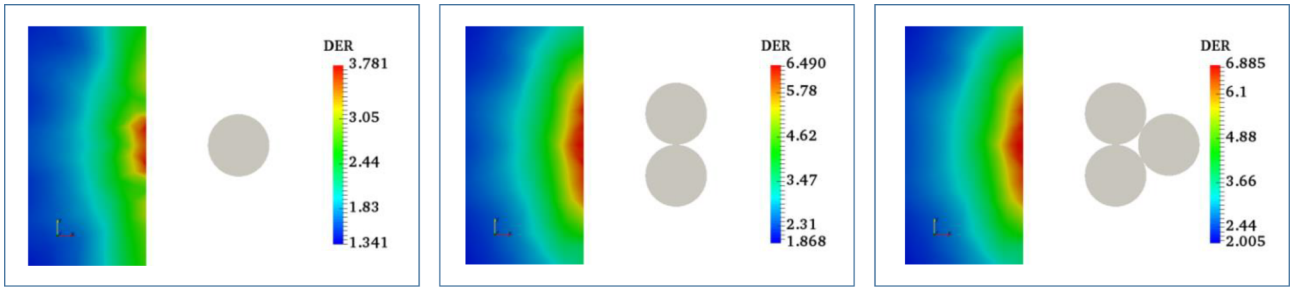

Fig. 3. DER profiles for a membrane thickness of 300 nm due to different GNP patterns detached from the septum, x-ray photons generated at 120 kVp are incident from the left.

4. Discussion

The main objective of this study was to investigate the feasibility of using GNPs as a radio-sensitizing agent in inhalational nanomedicine, and to assess the dosimetric effect of GNPs coating rupture. To this end, the deterministic radiation transport code SCEPTRE was used to quantitatively resolve the fine details of the DER profiles in the nanometric region around GNPs, when attached and detached from the alveolar septum. The nature of DER profiles and the formation of hot spots reveal significant clinical implications which are important in evaluating the biological impact of GNP-aided radiation therapy. As pointed out recently by Gadoue et al. [8], the presence of hot spots will result in important radiobiological consequences that could promote the radio-therapeutic benefit in cancer treatment. According to their study, hot spots provide a greater contribution to cell killing as a result of the increased radical creation. Additionally, the presence of hot spots not only improve the treatment outcome, but also implies a decreased risk of death, and a better quality of life for cancer patients, since the radiation dose has been increased as suggested by Machtay in his study [3].

An additional benefit that can be gained from boosting the dose delivered to the lung, via GNP inhalation, is the favorable sparing of healthy tissue, owing to the short range of DER profiles characteristic to GNP sensitization. According to the results, the values of DER for all examined cases drop below two after 300 nm within the membrane. This is in broad agreement with the work of many researchers, where it has been demonstrated that the energy deposition in the vicinity of nanoparticles is large, and that this effect is limited only to the microscopic vicinity of GNPs [6–10]. Preferably, this demonstrates threefold viability of using GNPs in theranostic inhalational nanomedicine. Firstly, they increase the radiation dose to the treatment site with a high degree of localization, while secondly, they decrease the risk of death and increase the quality of life of lung cancer patients, and thirdly, their short range effects help sparing the surrounding healthy tissue.

However, the aforementioned advantages could be lost due to the undesirable situation where the nanoparticles are detached from the surface of the septum, due to the rupture of the chemical bonds in the coating material. In this respect, the values of the DER and the concomitant hot spots will be greatly reduced, a condition that will lead to suboptimal outcome, due to the decreased dose amplification, and radical formation [8]. It is worth noting that the extent of such reduction mainly depends upon the separation distance between GNP(s) and the septum following coating inactivation. Arbitrarily, in this study, this distance is assumed to be 100 nm; however, it may be anticipated that a larger separation distance, which is quite probable in such circumstances, could lead to further reduction in the DER profiles.

Hao et al. [35] showed that a significant increase in the dose delivered to lung tumors can be achieved when nanoparticles are administered via the inhalation route. In their study, they used an approximate analytical method to calculate DER, by assuming a homogeneous distribution of nanoparticles and an isotropic emission of photo-electrons. However, GNPs form aggregates of different patterns when interacting with biomolecules [46]. More importantly, the photoelectron emission is anisotropic, and the angular distribution is given by Sauter or Fisher distribution, for relativistic and non-relativistic electron energies, respectively [43]. Gadoue et al. [7] investigated the angular anisotropy in the profiles of DER around GNPs when exposed to x-rays, and found that the degree of such non-uniformity is dependent on several factors such as GNP size, incident x-ray energy, and spectrum. Additionally, they pointed out that this angular variation is a function of the polar (or azimuthal) angle measured from the axis along which x-rays are incident. In the present work, the effects of anisotropy are prevalent in the DER profiles around the GNP, as reported by Gadoue et al. [7].

A remarkable feature of the results is that the maximum DER value in the hot spot region is not a linear function of the number of GNPs, irrespective of being attached or detached from the septum. For instance, the maximum DER value in the case of GNP attached to the membrane for three particles is 16.168, while it is 14.964 for an aggregate consisting of two particles, though one GNP has a maximum value of 9.998. On the other hand, these values are 6.885, 6.49, and 3.781 respectively for the detached case. Besides, according to Fig. 4, the values of DER along x-axis are not doubled nor tripled by increasing the number of GNPs to two or three, respectively. The non-linear relationship between the number of GNPs in a cluster and the resulting DER values is consistent with the results of Gadoue et al. [8]. In their study, they concluded that, due to the short range of Auger electrons whose the mechanism of GNP dose enhancement is strongly based on, adding a nanoparticle to an ensemble of GNPs does not result in a significant increase in the value of DER around the cluster.

Furthermore, the difference between the DER values of one and two GNPs is larger than it is between two and three GNPs in the attached case. In fact, the DER profiles of two and three GNPs are very close to each other, which imply that the contribution of the third GNP (not bound to the membrane) to the total enhancement is minimal due to the loss of a large fraction of its secondary electrons in air, or within the other GNP in the cluster, in addition to the short-term effects of Auger electrons. The abovementioned observation highlights the fact that the contribution of a GNP to the dose enhancement is not significant, unless it is bound to the membrane, not to the cluster of the GNPs.

In particular, DER profiles due to GNPs in the lung are characterized by the intricate behavior of secondary electrons at the interface between gold, air, and membrane tissue, due to the substantial dissimilarity in physical and dosimetric properties of these materials. Despite the fact that the results obtained in this study are for the specific purpose of GNPs inhaled in the lung, the insights gained from the findings can be extended to mostly all other organs and for other GNP administrations as well. However, for organs or tissues where air is not present, the effect of GNP detachment will be more pronounced. This can be attributed to the fact that the electronic stopping power of soft tissue is orders of magnitude greater than air. In this perspective, an increased loss of the secondary electrons emitted from the detached GNP can be seen in soft tissue, as compared to air. Henceforth, this will result in an exacerbated reduction of the enhancing capability of GNPs.

The main limitation of this study is the investigation of x-ray photons generated at 120 kVp as representative of only theranostic applications, while not examining therapeutic energy beams (MV). Nevertheless, the DER due to GNPs in the MV energy region is extremely small compared to kV beams [8,11–14,47]. Therefore, the choice of the incident photon energy is justified by the fact that therapeutic beams do not offer a comparable clinically noticeable benefit as theranostic x-rays. Another limitation is the use of a limited number of GNP clustering patterns. Indeed, the nanoparticles aggregates may consist of a varying number of GNPs and can take different shapes, yet the study was focusing on the basic clustering patterns. Furthermore, in the developed model, it has been implicitly assumed that the irradiation occurs while all nanoparticles are attached to the membrane. However, this may not be completely accurate since some particles may be free in the airways, but given the density of gold this scenario has a low probability.

This study presents a new consideration of the possible adverse dosimetric consequences of GNPs detachment from bio-surfaces. In the light of the results, one attached GNP is practically more effective than an ensemble of three GNPs detached from the membrane; a fact that prompts the necessity of careful scrutiny of the GNP coating properties and characteristics. More specifically, it must be ensured that the nanoparticle will latch on to the particular surface or membrane during the planned irradiation, thereby, achieving the maximal clinical benefit of the enhancing power of GNPs. Another important practical implication is the additional benefit of endocytosis targeting in nanoparticles-aided radiotherapy, since this mechanism will implicitly avoid

any possible complications related to GNP detachment and loss of enhancement capabilities. In the future, further studies, which examine a wider range of incident photon energies, need to be undertaken. Additionally, a more sophisticated lung model may be developed, and more complex scenarios could be investigated, such as the effect of free nanoparticles in the airways.

5. Conclusions

Using a next-generation deterministic coupled photon-electron radiation transport code with nanometric unstructured spatial mesh, detailed DER profiles were obtained at the interface between air, gold, and the septic membrane in the proposed lung model. The findings are quite convincing and, based on the results, it can be concluded that the inhalation of GNPs is beneficial in the treatment of lung cancer. The large values of DER in conjunction with the developed hot spots imply that this approach will have important radiobiological consequences in terms of cell killing. On the negative side, the study has investigated the possible scenario in which the same electrons required to enhance the dose around GNP might adversely disrupt the chemical bonds in the nanoparticle coating. After being detached from the membrane, the enhancing power of GNPs could be degraded by a factor that can approach 62%. Finally, a detailed knowledge of the DER profiles and adherence features is essential to improve the understanding of GNP sensitization properties, and to maximize the impact of GNP-aided radiation therapy.

Competing interests

The authors declare that they have no competing interests.

Funding

This research did not receive any specific grant from funding agencies in the public, commercial, or not-for-profit sectors.

Acknowledgments

The authors would like to thank Dr. Cliff Drum at Sandia National lab for his helpful advice and fruitful discussions about SCEPTRE. Thanks must also go to the physics department at the University of Massachusetts Lowell and GHPCC for providing the computational resources needed to run the simulations.

References

[1] www.cancer.org. cancer-facts-and-figures-2017.
[2] Keall PJ, Mageras GS, Balter JM, Emery RS, Forster KM, Jiang SB, et al. The management of respiratory motion in radiation oncology report of AAPM Task Group 76. Med Phys 2006;33:3874–900. https://doi.org/10.1118/1.2349696.
[3] Machtay M, Swann S, Komaki R, Byhardt R, Paulus R, Sause W, et al. Higher BED is associated with improved local-regional control and survival for NSCLC treated with chemoradiotherapy: an RTOG analysis. Int J Radiat Oncol Biol Phys 2005;63. https://doi.org/10.1016/j.ijrobp.2005.07.072. S40-S.
[4] Toomeh D, Gadoue SM, Yasmin-Karim S, Singh M, Shanker R, Singh SP, et al. Minimizing the potential of cancer recurrence and metastasis by the use of graphene oxide nano-flakes released from smart fiducials during image-guided radiation therapy. Phys Med 2018;55:8–14.
[5] Mehrnia SS, Hashemi B, Mowla SJ, Arbabi A. Enhancing the effect of 4MeV electron beam using gold nanoparticles in breast cancer cells. Phys Med. 2017;35:18–24. https://doi.org/10.1016/j.ejmp.2017.02.014.
[6] Mesbahi A. A review on gold nanoparticles radiosensitization effect in radiation therapy of cancer. Rep Pract Oncol Radiother 2010;15:176–80. https://doi.org/10.1016/j.rpor.2010.09.001.
[7] Gadoue SM, Toomeh D, Zygmanski P, Sajo E. Angular dose anisotropy around gold nanoparticles exposed to X-rays. Nanomedicine 2017;13:1653–61. https://doi.org/10.1016/j.nano.2017.02.017.
[8] Gadoue SM, Zygmanski P, Sajo E. The dichotomous nature of dose enhancement by gold nanoparticle aggregates in radiotherapy. Nanomedicine (Lond) 2018;13:809–23. https://doi.org/10.2217/nnm-2017-0344.
[9] Carter JD, Cheng NN, Qu Y, Suarez GD, Guo T. Nanoscale energy deposition by X-ray absorbing nanostructures. J Phys Chem B 2007;111:11622–5. https://doi.org/10.1021/jp075253u.
[10] McMahon SJ, Hyland WB, Muir MF, Coulter JA, Jain S, Butterworth KT, et al. Nanodosimetric effects of gold nanoparticles in megavoltage radiation therapy. Radiother Oncol 2011;100:412–6. https://doi.org/10.1016/j.radonc.2011.08.026.
[11] Lechtman E, Chattopadhyay N, Cai Z, Mashouf S, Reilly R, Pignol JP. Implications on clinical scenario of gold nanoparticle radiosensitization in regards to photon energy, nanoparticle size, concentration and location. Phys Med Biol 2011;56:4631–47. https://doi.org/10.1088/0031-9155/56/15/001.
[12] Jones BL, Krishnan S, Cho SH. Estimation of microscopic dose enhancement factor around gold nanoparticles by Monte Carlo calculations. Med Phys 2010;37:3809–16. https://doi.org/10.1118/1.3455703.
[13] Roeske JC, Nunez L, Hoggarth M, Labay E, Weichselbaum RR. Characterization of the theorectical radiation dose enhancement from nanoparticles. Technol Cancer Res Treat 2007;6:395–401. https://doi.org/10.1177/153303460700600504.
[14] Cho SH. Estimation of tumour dose enhancement due to gold nanoparticles during typical radiation treatments: a preliminary Monte Carlo study. Phys Med Biol 2005;50:N163.
[15] Fathy MM, Mohamed FS, Elbialy N, Elshemey WM. Multifunctional chitosan-capped gold nanoparticles for enhanced cancer chemo-radiotherapy: an invitro study. Phys Med 2018;48:76–83. https://doi.org/10.1016/j.ejmp.2018.04.002.
[16] Gatoo MA, Naseem S, Arfat MY, Dar AM, Qasim K, Zubair S. Physicochemical properties of nanomaterials: implication in associated toxic manifestations. Biomed Res Int 2014;2014:498420https://doi.org/10.1155/2014/498420.
[17] Nel A, Xia T, Madler L, Li N. Toxic potential of materials at the nanolevel. Science 2006;311:622–7. https://doi.org/10.1126/science.1114397.
[18] Aillon KL, Xie Y, El-Gendy N, Berkland CJ, Forrest ML. Effects of nanomaterial physicochemical properties on in vivo toxicity. Adv Drug Deliv Rev 2009;61:457–66. https://doi.org/10.1016/j.addr.2009.03.010.
[19] Verma A, Stellacci F. Effect of surface properties on nanoparticle–cell interactions. Small 2010;6:12–21.
[20] Champion JA, Mitragotri S. Role of target geometry in phagocytosis. Proc Natl Acad Sci USA 2006;103:4930–4. https://doi.org/10.1073/pnas.0600997103.
[21] Griffitt RJ, Luo J, Gao J, Bonzongo JC, Barber DS. Effects of particle composition and species on toxicity of metallic nanomaterials in aquatic organisms. Environ Toxicol Chem 2008;27:1972–8. https://doi.org/10.1897/08-002.1.
[22] Butterworth KT, McMahon SJ, Currell FJ, Prise KM. Physical basis and biological mechanisms of gold nanoparticle radiosensitization. Nanoscale 2012;4:4830–8. https://doi.org/10.1039/c2nr31227a.
[23] Liu Y, Liu X, Jin X, He P, Zheng X, Dai Z, et al. The dependence of radiation enhancement effect on the concentration of gold nanoparticles exposed to low- and high-LET radiations. Phys Med 2015;31:210–8. https://doi.org/10.1016/j.ejmp.2015.01.006.
[24] Müllner M, Schlattl H, Hoeschen C, Dietrich O. Feasibility of spectral CT imaging for the detection of liver lesions with gold-based contrast agents–a simulation study. Phys Med 2015;31:875–81.
[25] Huang X, El-Sayed MA. Gold nanoparticles: optical properties and implementations in cancer diagnosis and photothermal therapy. J Adv Res 2010;1:13–28.
[26] Khan I, Saeed K, Khan I. Nanoparticles: properties, applications and toxicities. Arab J Chem 2017.
[27] Ealia SAM, Saravanakumar M. A review on the classification, characterisation, synthesis of nanoparticles and their application. IOP Conference Series: Mater Sci Eng: IOP Publishing 2017:032019.
[28] Dobrovolskaia MA, Aggarwal P, Hall JB, McNeil SE. Preclinical studies to understand nanoparticle interaction with the immune system and its potential effects on nanoparticle biodistribution. Mol Pharm 2008;5:487–95. https://doi.org/10.1021/mp800032f.
[29] Bednarski M, Dudek M, Knutelska J, Nowinski L, Sapa J, Zygmunt M, et al. The influence of the route of administration of gold nanoparticles on their tissue distribution and basic biochemical parameters: in vivo studies. Pharmacol Rep 2015;67:405–9. https://doi.org/10.1016/j.pharep.2014.10.019.
[30] Alkilany AM, Murphy CJ. Toxicity and cellular uptake of gold nanoparticles: what we have learned so far? J Nanopart Res 2010;12:2313–33.
[31] Chen YS, Hung YC, Liau I, Huang GS. Assessment of the in vivo toxicity of gold nanoparticles. Nanoscale Res Lett 2009;4:858–64. https://doi.org/10.1007/s11671-009-9334-6.
[32] Cho EC, Xie J, Wurm PA, Xia Y. Understanding the role of surface charges in cellular adsorption versus internalization by selectively removing gold nanoparticles on the cell surface with a I2/KI etchant. Nano Lett 2009;9:1080–4. https://doi.org/10.1021/nl803487r.
[33] Lee WH, Loo CY, Traini D, Young PM. Inhalation of nanoparticle-based drug for lung cancer treatment: advantages and challenges. Asian J Pharm Sci 2015;10:481–9. https://doi.org/10.1016/j.ajps.2015.08.009.
[34] Lara Y, Nguyen T, Marilena L, Alexander M. Toxicological considerations of clinically applicable nanoparticles. Nano Today 2011;6:585–607.
[35] Hao Y, Altundal Y, Moreau M, Sajo E, Kumar R, Ngwa W. Potential for enhancing external beam radiotherapy for lung cancer using high-Z nanoparticles administered via inhalation. Phys Med Biol 2015;60:7035–43. https://doi.org/10.1088/0031-9155/60/18/7035.
[36] Taratula O, Garbuzenko OB, Chen AM, Minko T. Innovative strategy for treatment of lung cancer: targeted nanotechnology-based inhalation co-delivery of anticancer drugs and siRNA. J Drug Target 2011;19:900–14. https://doi.org/10.3109/1061186X.2011.622404.
[37] Taratula O, Kuzmov A, Shah M, Garbuzenko OB, Minko T. Nanostructured lipid carriers as multifunctional nanomedicine platform for pulmonary co-delivery of anticancer drugs and siRNA. J Control Release 2013;171:349–57. https://doi.org/

10.1016/j.jconrel.2013.04.018.
[38] Nakane H. Translocation of particles deposited in the respiratory system: a systematic review and statistical analysis. Environ Health Prev Med 2012;17:263–74. https://doi.org/10.1007/s12199-011-0252-8.
[39] Liang L, Larsen EW, Chetty IJ. An anatomically realistic lung model for Monte Carlo-based dose calculations. Med Phys 2007;34:1013–25. https://doi.org/10.1118/1.2437284.
[40] Schuemann J, Berbeco R, Chithrani DB, Cho SH, Kumar R, McMahon SJ, et al. Roadmap to clinical use of gold nanoparticles for radiation sensitization. Int J Radiat Oncol Biol Phys 2016;94:189–205.
[41] Williams RG, Gesh CJ, Pagh RT. Compendium of material composition data for radiation transport modeling. Richland, WA (US): Pacific Northwest National Laboratory (PNNL); 2006.
[42] Kramer R, Khoury HJ, Vieira JW, Lima VJ. MAX06 and FAX06: update of two adult human phantoms for radiation protection dosimetry. Phys Med Biol 2006;51:3331–46. https://doi.org/10.1088/0031-9155/51/14/003.
[43] Davisson CM, Evans RD. Gamma-ray absorption coefficients. Rev Modern Phys 1952;24:79–107. https://doi.org/10.1103/RevModPhys.24.79.
[44] Drumm CR. Spherical harmonics (PN) methods in the SCEPTRE radiation transport code. Albuquerque, NM, United States: Sandia National Laboratories (SNL-NM); 2015.
[45] Pautz SD, Bohnhoff WJ, Drumm CR, Fan WC. Parallel discrete ordinates methods in the sceptre project. Albuquerque, NM, United States: Sandia National Laboratories (SNL-NM); 2009.
[46] Basu S, Ghosh SK, Kundu S, Panigrahi S, Praharaj S, Pande S, et al. Biomolecule induced nanoparticle aggregation: effect of particle size on interparticle coupling. J Colloid Interface Sci 2007;313:724–34. https://doi.org/10.1016/j.jcis.2007.04.069.
[47] Gadoue SM, Toomeh D. Enhancement of linear energy transfer in gold nanoparticles mediated radiation therapy. Phys Med 2019. https://doi.org/10.1016/j.ejmp.2019.02.019.